AD-A246 889

PL-TR-91-2215

CRUSTAL AND UPPER MANTLE VELOCITY GRADIENTS IN THE VICINITY OF THE
EAST KAZAKH TEST SITE

Vernon F. Cormier
Michael D. Kalmbach

Department of Geology and Geophysics
University of Connecticut
Storrs, CT 06269-2045

DTIC
ELECTE
JAN 15, 1992
S B D

9 September 1991

92-01236

Scientific Report No. 1

92 1 14 018

The views and conclusions contained in the document are those of the authors and should not be interpreted as representing the official policies, either expressed or implied, of the Air Force or the U.S. Government.

This technical report has been reviewed and is approved for publication.

JAMES F. LEWKOWICZ
Contract Manager
Solid Earth Geophysics Branch
Earth Sciences Division

JAMES F. LEWKOWICZ
Branch Chief
Solid Earth Geophysics Branch
Earth Sciences Division

DONALD H. ECKHARDT, Director
Earth Sciences Division

REPORT DOCUMENTATION PAGE

Public reporting burden for this collection of information is estimated to average 1 hour per response, including the time for reviewing instructions, searching existing data sources, gathering and maintaining the data needed, and completing and reviewing the collection of information. Send comments regarding this burden estimate or any other aspect of this collection of information, including suggestions for reducing this burden to Washington Headquarters Services, Directorate for Information Operations and Reports, 1215 Jefferson Davis Highway, Suite 1204, Arlington, VA 22202-4302, and to the Office of Management and Budget, Paperwork Reduction Project (0704-0188), Washington, DC 20503.

1. AGENCY USE ONLY (Leave blank)	2. REPORT DATE 9 September 1991	3. REPORT TYPE AND DATES COVERED Scientific No. 1

4. TITLE AND SUBTITLE
Crustal and Upper Mantle Velocity Gradients in the Vicinity of the East Kazakh Test Site

5. FUNDING NUMBERS
PE 62101F
PR 7600 TA 09 WU AW
Contract F19628-90-K-0043

6. AUTHOR(S)
Vernon F. Cormier
Michael D. Kalmbach

7. PERFORMING ORGANIZATION NAME(S) AND ADDRESS(ES)
University of Connecticut
Department of Geology and Geophysics
Storrs, CT 06269-2045

8. PERFORMING ORGANIZATION REPORT NUMBER

9. SPONSORING / MONITORING AGENCY NAME(S) AND ADDRESS(ES)
Phillips Laboratory
Hanscom AFB, MA 01731-5000

Contract Manager: James Lewkowicz/LWH

10. SPONSORING / MONITORING AGENCY REPORT NUMBER

PL-TR-91-2215

11. SUPPLEMENTARY NOTES

12a. DISTRIBUTION / AVAILABILITY STATEMENT

Approved for public release;
Distribution unlimited

12b. DISTRIBUTION CODE

13. ABSTRACT (Maximum 200 words)

The Lg wave is simulated three dimensionally by ray methods, in homogeneous models of the crust with smooth variations in thickness. Variations typical of mountainous regions are utilized, and the effect of these variations is examined in detail. Ray modeling shows that Lg is strongly attenuated by propagation across the thickened crustal root found beneath mountain ranges. While variations in the width of the mountain root are found to be unimportant, variations in the width of transition between thin and thick crust strongly influence attenuation. Propagation paths across transition regions 100 km wide result in weak Lg while 200 km transitions cause very little Lg attenuation. Lg is found to propagate very efficiently within a mountain root, with amplitude increased slightly by lateral reflections. Propagation across mountain belts at angles from 90 to 20 degrees (relative to strike) is shown to cause strong attenuation at all angles, with no identifiable optimal path.

The technique is applied to a rough thickness model of the Central Asian crust and although attenuation is predicted, close comparison of the synthetics with earthquake recordings reveals discrepancies that can not be entirely explained by ray methods in a homogeneous crust. This

14. SUBJECT TERMS
Lg, synthetic seismograms, Central Asia

15. NUMBER OF PAGES
46

16. PRICE CODE

17. SECURITY CLASSIFICATION OF REPORT	18. SECURITY CLASSIFICATION OF THIS PAGE	19. SECURITY CLASSIFICATION OF ABSTRACT	20. LIMITATION OF ABSTRACT
Unclassified	Unclassified	Unclassified	SAR

CONT OF BLOCK 13:

suggests that a more accurate model of the crust is required, including variations in crustal Q, surface sedimentary layers in the basin regions and the large scale 3-D heterogeneities associated with the uplifted regions.

TABLE OF CONTENTS

iii

SUMMARY

This report describes a portion of a two year project titled "Crustal and Upper Mantle Gradients in the Vicinity of the Kazakh Test Sites and their Effects on Regional Discriminants." The objectives of this project are to investigate the effects of crustal structure, including the effects of velocity gradients, on the amplitude, frequency content, and decay with distance of regional seismic phases. To investigate the effects of velocity gradients, the locked mode method of seismogram synthesis is modified to incorporate the effects of velocity gradients within thick, vertically inhomogeneous layers. Crustal and upper mantle gradients in the vicinity of the Kazakh test sites will be modeled by comparing observed with synthetic seismograms computed by this method. The trial and error modeling will be supplemented by direct, linearized inversion of complete waveforms for crustal and upper mantle gradients. Particular emphasis will be placed on the effects of gradients on the Pn/Sn discriminant. Also included in this project is an effort to model the Lg phase by dynamic ray tracing and superposition of Gaussian beams in a laterally varying crustal waveguide. The effect of known surface topography and Moho topography inferred from the assumption of isostasy will be investigated for regional Lg paths from the Kazakh test sites.

Locked Mode Synthesis with Gradient Layers

Cormier et al. (1991) describe the modifications of the locked mode method needed to incorporate gradients within layers. Initial testing of the effects of gradients confirms earlier work that found strong effects on interference head waves, Pn, and Sn. In a pass band of a SP-WWSSN seismograph, however, the synthetic seismograms of the first 10 Rayleigh modes were found to be relatively insensitive to the details of crustal structure, including gradients within the crust. The gross characteristics of Lg in this pass band seem to be primarily sensitive to average crustal velocities and crustal thickness. Introduction of layers is not necessary unless there is compelling evidence for crustal discontinuities observed in the earlier time window of the regional seismograms in the form of refracted body waves and interference head waves.

Synthesis of Lg in 3-D Models by Dynamic Ray Tracing

Lg is synthesized as a sum of multiply critically reflected S waves in the crust. The crust has a constant P and S velocity overlying a homogeneous mantle. Topography of the Moho is correlated with given or known surface topography under the assumption of Airy isostasy. The synthetics include geometric spreading and complex reflection transmission coefficients. Intrinsic attenuation, Lg/Sn interactions, and scattering by fine scale heterogeneities within the crust are ignored. The starting assumptions are essentially the same as those used by Kennett (1986) in identifying gross effects of crustal thickness on Lg by plotting the bounce points of critically reflected S waves in the crust. Here, however, waveforms are calculated and effects of geometric spreading are included by dynamic ray tracing (e.g., Červený, 1985).

Results obtained in experiments with a hypothetical mountain range found Lg transmission to be only weakly dependent on the angle of the path with respect to the strike of the mountain range, but more strongly dependent on the width of the crustal transition. Transmission across

wider transition zones is more efficient because a shallower Moho dip reduces Lg leakage into the mantle. An upper bound on SV to SH conversion due to Moho topography was found for the case of sources and receivers within the mountain belt. The amount of SH energy, however, was too small to account for the equalization of Lg energy on all components of motion commonly observed from explosion sources.

In an experiment to test this approach against observed Lg data, we examined the data reported by Ruzaikin et al. (1977) for paths from receivers in the Tian Shan to sources in the Tibet Plateau. Source depths and radiation patterns are included from those published by Molnar and Chen (1983). Variations in Lg propagation are qualitatively predicted, including good agreement between observed and predicted Lg waveforms along paths having efficient transmission. The waveform agreement along weak paths is not as good. Transmission in the observed data is much weaker. We attribute the poorer comparison for the weak paths to the omission of intrinsic attenuation and/or basin interactions in the synthetic Lg's. Considering the results of Baumgardt (1991), the omission of basin interactions is probably the more serious effect. Since variations in surface topography are associated with strong variations in the distribution of sedimentary basins as well as with Moho topography, it is clear that Lg interactions with basins must be included in any ray based modeling. The omission of basin effects in forward modeling techniques may also explain the consistently greater mount of Lg blockage by mountain belts seen in observations compared to predictions.

Conclusions

Details of crustal structure do not seem to have much of an effect on the peak amplitude and coda length of Lg in the frequency band up to 1 Hz. This result suggests that an adequate model to explain the gross features of Lg consists of a homogeneous crust having a thickness and average shear velocity representative of particular paths. Ray/beam modeling of Lg as a sum of multiply, critically reflected S waves demonstrates that Moho topography can have a profound influence on the efficiency of Lg propagation. Comparison of predicted with observed Lg propagation suggest that near surface structure, such as sedimentary basins, must also be included together with Moho topography to completely explain the attenuation and efficiency of Lg propagation. Good qualitative comparison of Lg codas in the 1-2 Hz band along selected paths suggest that incorporation of finer scale three-dimensional structure in the Earth's crust may only be required to explain characteristics of Lg propagation in the frequency band above 1 Hz.

Future Lg work will be directed towards including the effects of basin structure in ray/beam modeling and the effects of finer scale crustal structure in ray/beam modeling. One possible approach would be to include the effects of fine scale structure by operators in in the (ω, k) domain estimated for individual S legs in the crust. These operators can be easily constructed in a plane layered crust. In a crust having fine scale variations in three dimensions, these operators can be estimated by finite difference calculations for single plane S waves incident at varying take-off angles on the Moho.

RAY MODELING OF Lg WAVE ATTENUATION ACROSS MOUNTAINOUS REGIONS

Michael D. Kalmbach and Vernon F. Cormier

Department of Geology and Geophysics

University of Connecticut

Storrs, CT 06269-2045

August 1991

1

INTRODUCTION

First described by Press and Ewing (1952), the Lg phase propagates at crustal shear wave velocity, is recorded on all three seismometer components and can travel long distances with relatively small levels of attenuation. The last property is very useful in that it allows for detection of seismic events (earthquakes and underground nuclear tests) of very low magnitude.

Lg propagates efficiently within continental crust of near constant thickness, but propagation efficiency is strongly diminished by variations in thickness. Thickness variations occur in mountainous regions, where isostatic compensation leads to roots of thickened crust. Variations also exist in the transition regions between thick continental crust and thin oceanic crust. It has long been known that Lg is extinguished by propagation through as little as 100 kilometers of ocean crust (Press and Ewing, 1952).

A comprehensive understanding of the means of Lg attenuation is still lacking. Researchers have attributed attenuation to transmission (leakage) of body waves to the mantle, redistribution of surface wave energy to the deep crust and mantle, low Q (high intrinsic attenuation) and scattering within the heterogeneous crust associated with regions of extensive faulting, igneous intrusion and irregular layering. It is likely that each effect is important to some degree and that no single effect is responsible for all observed attenuation.

Forward modeling techniques been applied to the Lg attenuation problem to help in understanding how the wave propagates and to learn what surface recordings of Lg can tell us about the seismic source and the composition of the crust. Two mathematical descriptions, which are essentially equivalent, are useful in the forward modeling of Lg: rays and modes. From the ray

perspective, Lg is a channel wave, consisting primarily of S-wave reverberations between the free surface and the Moho. Rays incident at the Moho at angles greater than the critical angle of refraction lose no energy to the mantle, explaining why Lg is recorded strongly at great distances. Rays provide a quick method for examining Lg propagation through 3-D models of the crust. The modal explanation of Lg consists of high order surface modes with energy distributed throughout the crust. Modal representations, while useful in 1-D media for understanding regions of propagation, become more difficult to use in 2-D and 3-D media because of the computational expense of calculating mode coupling coefficients. Kennett (1986) gives a good general description of the Lg wave, in terms of both rays and modes.

The present study assumes the Lg explanation of shear waves reverberating within the entire crust and examines attenuation caused by transmission to the mantle and geometric spreading. Lg propagation is simulated by ray methods through mountainous regions and the results are presented in the form of synthetic short period seismograms. The crust is represented as a homogeneous medium of variable thickness. This approach is first applied across a hypothetical mountain range to predict attenuation levels under various conditions; propagation paths from perpendicular to near parallel and receiver locations before, within and beyond the transition regions. In subsequent tests, the mountain belt is made wider then given more gradual transition regions to judge the effects of these variations. Finally, Lg is simulated through a homogeneous model of the Central Asian crust and the results are compared to actual recordings to provide a measure of accuracy.

3

OBSERVATIONS OF Lg ATTENUATION

Lg wave attenuation is well documented in the geophysical literature. Review of these studies shows that strong attenuation is attributable to three causes: waveguide variations, backscattering by 3-D heterogeneities and intrinsic attenuation. Since the present study is concerned with waveguide (i.e.. the entire crust) variations, similar previous research is closely examined.

A study of seismic energy radiation from underground nuclear explosions and small-magnitude earthquakes (Sutton et. al., 1967) shows clear correlation between Lg wave energy and the tectonic provinces of the United States. Iso-energy lines closely parallel the eastern front of the Rocky mountain range for events occurring both to the east and to the west of the front, indicating a strong attenuation gradient. The symmetry would seem to rule out intrinsic attenuation as a major factor, leaving waveguide variation and scattering attenuation as possible explanations.

Ruzaikin et. al. (1977) study Lg wave propagation in mountainous regions of central Asia and find strong Lg attenuation for certain propagation paths. Specifically, earthquakes occurring within the Himalayas and Tibetan Plateau and recorded in the lower surrounding regions generally have weak or non-existent Lg. A particular fault within the Tibetan Plateau seemed to have a strong affect on the recordings, as propagation paths crossing this fault result in weak Lg displacement but similar paths that do not cross the fault provide much stronger Lg. Disruption or elimination of the crustal waveguide and variations in Q are proposed as explanations. although the authors disagree on the importance of the individual factors. An analysis of this region by Kennett (1986) notes that there are sharp boundaries well within the Tibetan Plateau separating events for which Lg is recorded or not recorded. The interpretation is given in terms of the range of emergence

angles or equivalently, phase velocities, of direct S-waves. Events occurring close to the transition from thick to thin crust provide direct waves that may travel at relatively steep angles (high phase velocity). These waves undergo conversion to the higher order Rayleigh and Love modes with energy distributed throughout the crust that are characteristic of Lg. With increasing distance from the transition, direct waves travel at shallower angles, and at a critical distance corresponding to direct wave phase velocity of 3.45 km/sec, Lg disappears. The shallow emergence body waves convert only to low order modes, which at high frequency have energy confined to near surface sediments.

Shishkovich (1979) reports that Lg is attenuated when crossing mountain ranges and that attenuation is greater when propagation angles are more oblique (relative to the predominant strike of the mountains). Noponen and Burnetti (1980) examine Lg wave propagation in Alaska and find that Lg is unexpectedly weak when the propagation path crosses a portion of the Denali fault.

Lg wave propagation near Denmark and the North Sea is studied by Gregersen (1984) and although a distinct pattern of attenuation is observed, comparison between propagation paths through bedrock regions versus paths through regions with 8-10 km of sediments finds no significant differences. It is suggested that deep crustal anomalies, possibly variations in crustal thickness, are responsible for the observed Lg wave attenuation. Kennett and Mykkeltveit (1984) observe that Lg is almost entirely extinguished when propagation paths cross the North Sea central graben and attribute the strong attenuation to the crustal thinning associated with the graben structure. Maupin (1989) uses the first 11 Rayleigh and Love modes to model Lg as surface waves crossing

5

the North Sea central graben. Significant attenuation is predicted, but not enough to explain the observed near extinction. Deep crustal faulting and basaltic intrusions known to exist in the graben region are proposed to explain the discrepancy.

Lg transverse (Love) surface modes are modeled through the transition zone between continental and oceanic crust by Regan and Harkrider (1989) and the waveguide variation effects are analyzed. Crustal thinning at the transition from continent to ocean is found to cause an increase in modal energy at the surface along with an increase in coda duration. Simultaneously, energy is lost in the deep crust by conversion to mantle body waves. At the transition from oceanic to continental crust, surface amplitude decreases as the energy trapped in the oceanic crust is spread throughout the thickened crust. Their modeling predicts strong Lg attenuation, but as with other studies, the predicted levels are insufficient to explain the observed extinction of Lg through such regions.

In summary, crustal waveguide variations are believed to exert a strong attenuating effect on the Lg wave, but quantitative modeling studies have been unable to attribute all observed attenuation to waveguide effects alone. Scattering and intrinsic attenuation also appear capable of diminishing Lg, and may be required to accurately model the physical observations.

SOURCE MODELS

Three types of seismic sources were investigated in the course of this study: (1) shallow explosive sources with far-field displacement spectra estimated by the model of of Mueller and Murphy (1971); (2) shallow point double couples, assuming the theory of Brune (1970) for the far-field displacement spectra; (3) and horizontal and vertical point forces having having time dependence consistent with

6

either the far-field explosion model (1) or earthquake model (2).

Confined explosive sources couple into the surrounding rock primarily through compressional waves. Shear waves may be generated by multiple scattering in the source region, P to S wave conversion, tectonic stress release, spall and slapdown, and three dimensional heterogeneity along the propagation path (Kennett, 1989). Of these factors, only P to S wave conversion is easily modeled by ray methods and by Snell's law, S wave conversions at near horizontal boundary surfaces are too steep to account for the Lg reverberations. It is important to note that even at short distance from an explosive source, Lg energy is equalized on all components of motion, including the transverse. Since an explosive source cannot generate any SH, the transverse energy must be acquired from scattering heterogeneities within the waveguide and/or scattering at rough waveguide boundaries. Much evidence exists that source properties exert less influence on Lg attenuation than the crust through which Lg propagates, e.g., the similarity in attenuation patterns of earthquakes and explosions observed by Sutton et al., 1967. For these reasons, most of the examples shown in this paper have been computed for the radiation patterns of vertical or transverse point sources. The amount of transverse Lg obtained from the calculations with a vertical point force can be used to quantify the contribution of long wavelength (greater than 10 km) topography of the waveguide on SV to SH conversion. In the absence of a method to account for the effects of scattering by small scale heterogeneities within the waveguide, realistic Lg wavetrains can be simulated by assuming two othorgonally oriented point forces.

CRUSTAL MODELS

The crustal models are homogeneous, i.e., seismic wave velocity and density are constant throughout the crust. The homogeneous models do not account for all raypaths that would exist in layered models nor do they account for bending of rays within a crust with smooth velocity gradients. The effects of neglecting layering and velocity gradients are discussed in RESULTS section. The mantle is a half-space, with rock properties defined only at the crust- mantle boundary. Since body wave propagation within the Since mantle is not considered, mantle properties are only used for calculation of reflection coefficients and phase shift. The crust is 3-dimensional, which is required for simulation of arbitrary Lg paths through mountainous regions.

The boundary surfaces that form the Lg waveguide are the free surface and the crust-mantle boundary or Moho. It is important that an accurate technique is used for surface representation, because the effects of these variations is the main result of the present study. Three dimensional surfaces are commonly modeled numerically using interpolation algorithms. Surfaces are represented by values (depth for instance) at mesh points and surface values between mesh points are found by interpolation. Three interpolation algorithms were evaluated. Bilinear interpolation is very fast computationally and provides a reasonable fit, but the discontinuities in first and second derivatives (slope and curvature) at mesh points is an artificial property, and the diffraction effect of these points is not properly modeled by the ray method. Bicubic interpolation uses bicubic polynomials to interpolate and allows second derivatives to be specified at the mesh points. The discontinuities at mesh points are then removed, but this algorithm was found to be computationally expensive compared to the bilinear method. Bicubic spline interpolation again uses bicubic

polynomials and matches curvature at mesh points, but the automatic selection of curvature leads to unrealistic surfaces. Variations on the basic spline interpolation might provide better results. Bicubic interpolation was chosen from the three because it allows for accurate surface representation and is consistent with ray modeling, as long as care is taken that radius of surface curvature is much larger than wavelength.

The material properties (table 1) are those used in the homogeneous model of Bouchon (1982). Mantle properties match PREM (Dziewonski and Anderson, 1981) within 5 percent. Because the actual crust is far from homogeneous, crustal properties are taken as average values.

SYNTHETIC SEISMOGRAMS

Synthetic seismograms are calculated from the superposition of elementary waves, with each wave represented by a two- point raypath. Complex reflection transmission coefficients are included as is geometric spreading by the methods summarized in Červený et al., (1977). Since rays approach the seismometer from various incidence and azimuthal angles, recorded ground displacement is found by rotation of displacement from ray centered coordinates to the coordinates of the seismometer. Convolution of displacement with the WWSSN short period seismometer response gives the synthetic seismograms.

9

RESULTS

Propagation in a Planar, Homogeneous Waveguide

The cross-sectional ray diagrams of Figure 1 show rays travelling at the Lg velocity range from a near surface source. For clarity, ray sampling is sparse and only downgoing rays are shown. In 1a, the waveguide boundaries are planar and horizontal. Ray parameters do not change on reflection and no energy is lost to mantle transmission or S to P wave conversion. Geometric spreading and intrinsic and scattering attenuation determine the strength of Lg and if the attenuating factors are low, Lg will be a prominent seismogram feature.

Lg rays across a mountain root are illustrated in Figure 1b. This is a condition of attenuation and several effects are apparent. The dipping transition to thicker crust reflects rays at shallower angles and introduces a shadow zone to the right of the transition. This transition causes no energy loss to the mantle because reflections are still at post- critical angles. At the transition to thinner crust, ray angles become steeper and body waves are transmitted to the mantle both at and beyond the transition zone. Geometric spreading is related to ray density, so the density of rays in the diagram provides a qualitative measure of amplitude.

Figures 2a and 2b show Lg wave displacement and the corresponding synthetic seismogram from a near surface transverse point source and source-time spectrum characteristic of a 100 kiloton explosion (see SOURCE MODELS). The offset is 1000 km. The crust has plane horizontal boundaries at the free surface and the Moho. Crust and mantle density and S and P wave velocities are given in table 1. Certain basic characteristics of Lg are evident, as well as an important modeling deficiency. The traces are composed of a series of high frequency pulses, as is the case

10

with the Lg wave. The group velocity window of significant energy is between 3.52 km/sec to 2.89 km/sec, in good agreement with Lg observations. The primary difficulty with these traces involves the flat periods between pulses. Ground motion is generally continuous in observed Lg, and this aspect has not been recreated. Bouchon (1982) found similar results for the case of a homogeneous crust, but was able to recreate Lg quite accurately with crustal models containing horizontal layers. Another method for calculating more realistic synthetics is to approximate the effects of scattering heterogeneities, giving each elementary pulse a short coda.

The major simplification made in the present study is that of a homogeneous crust. A layered model leads to more complicated seismograms because of the many additional rays created by reflection and reverberation within the crustal waveguide. These reflections and reverberations merely redistribute energy, they do not add to or detract from total energy within the crust. If layer boundaries are roughly horizontal, ray parameters remain constant and it is material properties in the bottom layer only that control attenuation by mantle transmission. Velocity and density in this layer can be matched equally well with homogeneous or layered models, so neglecting horizontal layering will not effect the attenuation results. If layer boundaries are not horizontal, ray paths may be drastically changed and attenuation may occur that is not predicted by the simplified modeling. Other forms of 3-D crustal heterogeneity, e.g., faults and intrusions, that are not included in the model may lead to similar errors in attenuation prediction.

The crust may also be modeled with smooth variations and a common representation is that of increasing velocity and density with depth. Rays traced through this type of model will have curved trajectories that are concave upward. With the exception of the upper 1 to 2 km of the

11

crust, realistic velocity gradients are weak and ray curvature is slight, with changes in vertical ray angle typically on the order of one of degree. Improvements compared to the homogeneous model are expected to be minimal, particularly if the homogeneous velocity and density match conditions at the crust-mantle boundary.

Propagation Perpendicular to a Mountain Range

Lg is modeled by summing rays in a laterally varying crustal waveguide simulating a hypothetical mountain range. Crustal thickness contours are shown in map view in Figure 3a. Certain characteristics, such as the square corners of the contour lines, are concessions made for modeling simplicity and are not expected to greatly influence the results. Background crustal thickness is taken as 35 km, which represents continental crust slightly elevated above sea level. The thickness of the mountain root is 50 km, which is consistent with gravity surveys in various high mountainous regions (e.g. Press, 1982, p. 437). A physical analogy to this model may be found in the South American Andes, which is similarly a narrow range with abrupt fronts on both sides.

Tested propagation paths are shown in Figure 3a and ray synthetic seismograms in Figure 3b for a vertical point force. The first trace shows Lg at the same offset as receiver R_1 through an undisturbed waveguide. Traces 2 through 4 are recordings from receiver locations R_1 through R_3. Visual comparison of the traces gives a measure of attenuation and the extensive numerical data from the program runs explain the primary cause (mantle transmission and/or defocusing). The seismogram from location R_1 shows that early Lg arrivals have high amplitude but later arrivals are considerably weaker. The effects of crustal thinning are not evident at this location and the weaker signal is explained entirely by propagation across the transition to thicker crust. The method of

attenuation is defocusing. The slower ray paths reaching location R_1 are reflected in areas of Moho curvature and as a result, average geometric spreading is increased by a factor of 2. Since Moho curvature is found to cause attenuation in this and other program runs, it is useful to consider an alternative transition model; a planar dipping Moho. The planar surface will not cause the increase in geometric spreading noted above, but will result in attenuation through other means. Specifically, much of the defocused energy that reaches the receiver through curved transitions is reflected by planar transitions in directions that do not reach the receiver. This is easily visualized by considering rays tubes and the area between rays, which is the wavefront. Defocusing leads to larger wavefronts which have a better chance of reaching the receiver than do the smaller wavefronts reflected by planar surfaces. The present study has compared the methods and found comparable levels of attenuation, although the seismograms are somewhat different in appearance.

A very slight increase in attenuation is evident at receiver location R_2, primarily because all rays reaching this point are defocused to some extent. Attenuation at location R_3 is quite a bit stronger than at R_1 and R_2. Here the propagation path crosses the transition to thinner crust, which diverts much of the energy that would otherwise reach the receiver. Diversion occurs in three ways. First, rays travelling at post-critical angles relative to the horizontal Moho become pre-critical at the upward dipping transition, and energy is lost to mantle transmission. Secondly, a large portion of the remaining reflected energy travels at pre-critical angles, leading to mantle transmission beyond the transition. The third method of diversion is back-reflected rays.

13

Propagation Perpendicular to a Mountain Range

Figure 4 illustrates the results of tests of Lg propagation parallel to the strike of a mountain range for a vertical point force. Sources and receivers are assumed to lie within a mountain range having a deep crustal root. Seismogram trace 1 shown again for reference propagation in a crust having planar free surface and Moho. Traces 2-4 correspond to receiver locations R_1, R_2 and R_3. Transition zones trending parallel to the propagation path form a secondary waveguide and the modeling predicts that rays will be trapped within. These raypaths are weak, however, as Moho curvature causes significant attenuation by geometric spreading. The seismogram at location R_1, which is not subject to transitions perpendicular to propagation, shows energy roughly equal to undisturbed Lg. Although a large number of raypaths with lateral reflections were traced, the increased geometric spreading leads to weak arrivals. The traces at locations R_2 and R_3 are seen to be strongly attenuated by the crustal thinning transition.

Rays trapped by the lateral waveguide undergo conversion between SV and SH, but conversions of this type are not noticeable in the synthetic seismograms. It is possible that because these rays tend to be weak, the conversions are not noticeable. Another possibility is that SH to SV conversion is generally canceled by SV to SH conversion under the particular conditions of this model. In the real crust, the primary method of SV to SH conversion is scattering by small scale heterogeneities, which can not be considered under the constraints of ray theory.

14

Propagation Oblique to a Mountain Range

Figure 5 illustrates the attenuation of Lg for paths oblique to the strike of a mountain range for a vertical point force. Sources and receivers are located such that propagation paths are at 90, 70, 45 and 20 degrees relative to the waveguide perturbations. Receiver distance is 2000 km in all cases. Strong attenuation is evident over each propagation path, but the individual waveforms vary considerably. For paths terminating at receivers R_1 and R_2, rays encounter steep thickness transitions and many rays are entirely transmitted to the mantle. Along the more oblique paths leading to R_3 and R_4, the Moho dips less steeply and as a result, the number of two-point ray paths increases. It appears that Lg propagates slightly more efficiently at 45 degrees than at the other angles tested, but the difference is insignificant compared to the level of attenuation.

Synthetic Lg seismograms from program run 4, which traces Lg through the crustal models of Figure 3a, 6a and 6b, are shown in Figure 6c. The base mountain range is first made wider with no change in the transitions then given more gradual transitions with in no change in width. Propagation paths are perpendicular and 2000 km in length. Traces 2 and 3, which compare a 200 km width of thickened crust with a 500 km width, both show weak Lg. The similarity between traces suggests that the width of a mountainous region has very little effect on overall attenuation. Trace 4 shows Lg after propagation through transition regions 200 km wide (compared to 100 km wide in trace 2) and the difference is readily apparent. The widened transition width results in Lg amplitude analogous to that in the undisturbed waveguide, which implies that the width of crustal transition regions and the corresponding change in overall Moho dip angle impose the primary control over Lg attenuation.

15

Example: Propagation Across the Tibet Plateau

The map shown in Figure 7a gives source and receiver locations used in the Lg analysis of Ruzaikin et. at., 1977. Shading corresponds to regions of high mountains. Central Asia was chosen to test the methods of the present study because Lg is known to be highly attenuated here and good specific examples are given in published seismograms. A study of focal mechanisms in the Tibetan Plateau (Molnar and Chen, 1983) found these earthquakes to occur at depths of 5 to 10 km with combined strike-slip and normal faulting and T axis primarily east-west. No earthquakes were located below 10 to 15 km, suggesting the crust is essentially aseismic below these depths. The fault solutions indicate the Tibetan Plateau is undergoing east-west extension, much like the Basin and Range province of the Western United States.

Crustal thickness has been put into a digital model and the results, in the form of a Moho depth plot, are shown in Figure 7b. Samples are taken every 87 km of longitude and every 54 km of latitude, which corresponds roughly to 1 degree by .5 degree sampling. The method of determining crustal thickness is a combination of published survey results and inference. Choudary, 1975 estimates crustal thickness of 70-72 km in the Central Himalayas from Bouger gravity anomalies. Bird and Toksoz, 1975 study the velocity of 20-80 second Rayleigh waves and conclude that the crust is 75 km thick within the Tibetan Plateau. Published data on crustal thickness within the Tarim Basin and Tien Shan Mountains were not found, so thickness has been estimated from average elevation. Elevation varies from 500 to 1000 meters within the Tarim Basin and crustal thickness is estimated at 35 km. Average Tien Shan elevation is on the order of 3000 meters, leading to a thickness estimate of 50 km. Estimation of crustal thickness combined with the large digital

16

sampling intervals lead to a very rough model of the crust, but the transitions, which seem to most strongly effect Lg propagation, are represented as closely as the model will allow.

Figure 7a shows propagation paths from the two earthquakes chosen for modeling by the ray method. Double couple radiation patterns have been included. Both paths are subject to crustal thinning at the Tarim Basin then crustal thickening at the Tien Shan mountains before the waves are recorded at Soviet station Talgar (TLG). Since the paths are similar, transition steepness will be approximately the same. The main difference between paths is that the leftmost path travels about half as far within the Tibetan Plateau. Seismograms recorded from the left earthquake (mb=5.1) are shown in Figure 8a. Traces TLG a and b are sensitive to 1.25-2.0 second and 2.5-5.0 second periods respectively and Lg wave energy is apparent on both traces. Figure 9a shows seismograms from the right earthquake (mb=6.1) and Lg appears to be very weak in these recordings. We then have a strong path and a weak path to which ray modeling may be applied. Figure 8b is a synthetic seismogram over the strong path and Figure 9b is the synthetic of the weak path. Top traces are again used for reference. The synthetic trace of the strong path shows significant attenuation, which is likely accurate since actual Lg amplitude is not much higher than at Pn and Pg traveltimes. The synthetic seismogram of the weak path shows about the same level of attenuation, which corresponds with the earlier finding that propagation distance within thickened homogeneous crust does not control attenuation levels, but contradicts the evidence of the recorded seismograms.

It appears then that ray modeling in a homogeneous crust can not entirely explain attenuation within this region. Certain additions to the crustal model could significantly improve the match

17

between the synthetics and the recordings. First, inclusion of the low Q believed to exist in the deep crust of the Tibetan Plateau (Bird and Toksoz, 1975) would improve correlation. Each ray incident at the Moho beneath the Tibetan Plateau would be subject to high intrinsic attenuation, establishing a direct relationship between travel distance within the plateau and attenuation. Scattering attenuation by the 3-D heterogeneities associated with the uplifted region would tend to reinforce this relationship. These improvements over the homogeneous crust alone may be sufficient to provide an acceptable match between synthetics and recordings, but we can go a step further, and following the argument of Kennett (1986), assume that it is primarily the direct rays emerging from the Tibetan Plateau that are energetic enough to excite Lg outside the plateau. The model of the Tarim Basin crust should then be modified to include it's surface sedimentary layer. Low seismic velocity within the sediments would form a waveguide trapping all rays with shallow emergence. Rays in the sedimentary waveguide would not propagate as efficiently as those reverberating within the entire crust because of high levels of scattering attenuation within the sediments. It is believed that these modeling improvements could lead to synthetics that closely match the attenuation levels seen in the recorded seismograms. Recent work of Baumgardt (1991) has confirmed the importance of low velocity sedimentary basins in explaining Lg attenuation. For the paths he investigated from Soviet Central Asia to northern Europe, Baumgardt found that the effect of Moho topography was insignificant. In contrast, variation in sedimentary basin structure along the paths seemed to be strongly correlated with variations in the efficiency of Lg propagation. In the example discussed here, however, Moho topography is likely to be as least as strong an effect as sedimentary basin structure. The strongest Moho topography in the paths investigated

18

by Baumgardt was associated with the inferred root of the Urals, which is much weaker than the surface and inferred Moho topography along the boundaries of the Tibet Plateau.

CONCLUSIONS

Ray methods applied to a homogeneous crust with 3-D curved boundaries is a useful method for modeling Lg propagation efficiency. While the synthetics fail to totally explain observations in Central Asia, they are in general agreement in that they do predict strong attenuation. This indicates that even the simple homogeneous model is valid to some extent in predicting Lg attenuation and that crustal waveguide effects alone strongly influence Lg. The specific recommendations for more accurate crustal models (inclusion of sedimentary layers, large scale 3-D heterogeneities and crustal Q), should lead to more accurate results in future studies of Lg.

Two specific results seem particularly useful. The first, that the angle at which Lg approaches mountainous regions has little effect on the predicted attenuation, would tend to validate studies in which lateral waveguide variations are neglected. The second result, that width of transition zones strongly influence attenuation, appears to be a new criteria for evaluation of Lg attenuation.

Details of crustal structure do not seem to have much of an effect on the peak amplitude and coda length of Lg in the frequency band up to 1 Hz., e.g, Cormier et al., (1991). result suggests that an adequate model to explain the gross features of Lg consists of a homogeneous crust having a thickness and average shear velocity representative of particula. paths. Ray/beam modeling of Lg as a sum of multiply, critically reflected S waves demonstrates that Moho topography can have a profound influence on the efficiency of Lg propagation. Comparison of predicted with observed

19

Lg propagation suggest that near surface structure, such as sedimentary basins, must also be included together with Moho topography to completely explain the attenuation and efficiency of Lg propagation. Good qualitative comparison of Lg codas in the 1-2 Hz band along selected paths suggest that incorporation of finer scale three-dimensional structure in the Earth's crust may only be required to explain characteristics of Lg propagation in the frequency band above 1 Hz.

ACKNOWLEDGEMENTS

REFERENCES

Baumgardt, D.R., (1991). High frequency array studies of long range Lg propagation and the causes of Lg blockage and attenuation in the Eurasian continental craton, Final Report, PL-TR-91-2059(II), Phillips Laboratory, Hanscom AFB, MA. ADA236984

Bird, P. and M.N. Toksoz (1975). Structure and evolution of the Tibetan Plateau, *EOS, Trans. Am. Geophys. Union 56*, 397.

Bouchon, M. (1982). The complete synthesis of seismic crustal phases at regional distances, *J. Geophys. Res. 87*, 1735-1741.

Červený, V., I.A. Molotkov and I. Pšencik (1977). Ray method in seismology. Univerzita Karlova.

Choudary, S.K. (1975). Gravity and crustal thickness in the Indo-Gangetic Plains and Himalayan region, India, *Geophys. J. R. Astr. Soc. 40*, 441-452.

Cormier, V.F., B. Mandal, and D. Harvey (1991). Incorporation of velocity gradients in the synthesis of complete seismograms by the locked mode method, *Bull. Seis. Soc. Am., 81*, 897-930.

Dziewonski, A.M. and D.L. Anderson (1981). Preliminary Reference Earth Model, *Physics of the Earth and Planetary Physics 25*, 297-356.

Gregersen, S. (1984). Lg-wave propagation and crustal structure differences near Denmark and the North Sea, *Geophys. J. R. Astr. Soc. 79*, 217-234.

Kennett, B.L.N. and S. Mykkeltveit (1984). Guided wave propagation in laterally varying media - II. Lg-waves in North-western Europe. *Geophys. J. R. Astr. Soc. 79*, 257-267.

Kennett, B.L.N. (1986). Lg waves and structural boundaries, *Bull. Seism. Soc. Am. 76*, 1133-144.

Kennett, B.L.N. (1989). On the nature of regional seismic phases - I. Phase representations for Pn, Pg, Sn and Lg, *Geophys. J. Int. 98*, 447-456.

Maupin, V. (1989). Numerical modelling of Lg wave propagation across the North Sea Central Graben, *Geophys. J. Int. 99*, 273-283.

Molnar, P. and W. Chen (1983). Focal depths and fault plane solutions of earthquakes under the Tibetan Plateau, *J. Geophys. Res. 88*, 1180-1196.

Mueller, R.A. and J.R. Murphy (1971). Seismic characteristics of underground nuclear detonations part I. Seismic spectrum scaling,*Bull. Seism. Soc. Am. 61*, 1675-1692.

Noponen, I. and J. Burnetti (1980). Alaskan regional data analyses, in "Study of seismic wave characteristics at regional distances", Teledyne-Geotech Report AL-80-1, Teledyne-Geotech, Alexandria, Virginia.

Press, F. and M. Ewing (1952). Two slow surface waves across North America, *Bull. Seism. Soc. Am.* *42*, 219-228.

Press, F. and R. Siever (1982). Earth, W.H. Freeman and Co.

Regan, J. and D.G. Harkrider (1989). Numerical modelling of SH Lg waves in and near continental margins, *Geophys. J. Int. 98*, 107-130.

Ruzaikin, A.I., I.L. Nersesov, V.I. Khalturin and P. Molnar (1977). Propagation of Lg and lateral variations in crustal structure in Asia, *J. Geophys. Res. 82*, 307-316.

Shishkovich, C. (1979). Propagation of Lg seismic waves in the Soviet Union, Rand Note, Santa Monica, California.

Sutton, G.H., W. Mitronovas and P.W. Pomeroy (1967). Short- period energy radiation patterns from underground nuclear explosions and small-magnitude earthquakes, *Bull. Seism. Soc. Am. 57*, 249-267.

Table 1. Homogeneous Crust and Mantle Properties

Layer	α (km/sec)	β (km/sec)	ρ (gm/cm^2)
Crust	6.30	3.65	2.90
Mantle	8.20	4.70	3.30
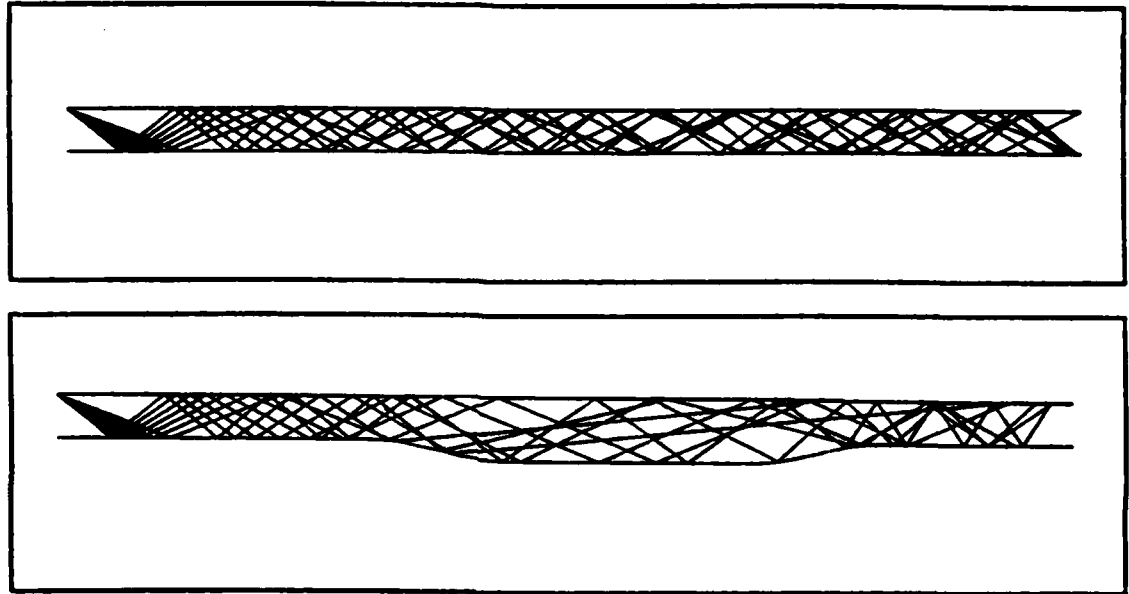
Figure 1: (a) Above: Lg ray diagram in a crust bounded by planar, horizontal free surface and Moho. Lg attenuation by leakage into the mantle halfspace is minimized under these conditions. (b) Below: Lg rays through a perturbed crust. Over 100 km transition regions, crustal thickness varies from 35 km to 50 km. The thicker crust represents a mountain root caused by isostatic compensation. The cross-section of the crust is drawn to scale showing that Moho topography changes much more dramatically than surface topography.

23
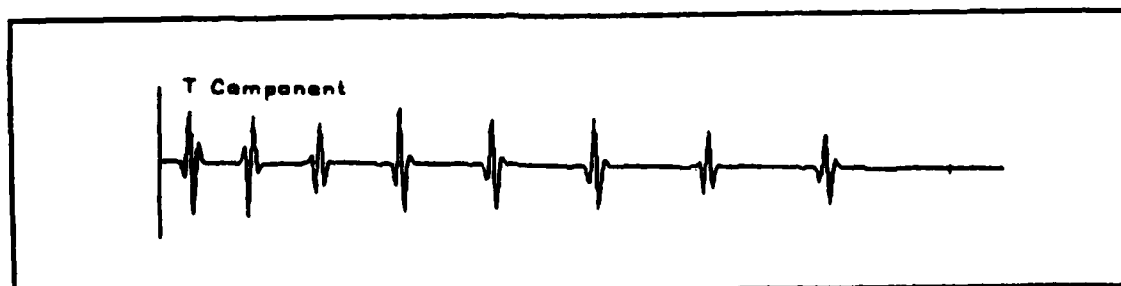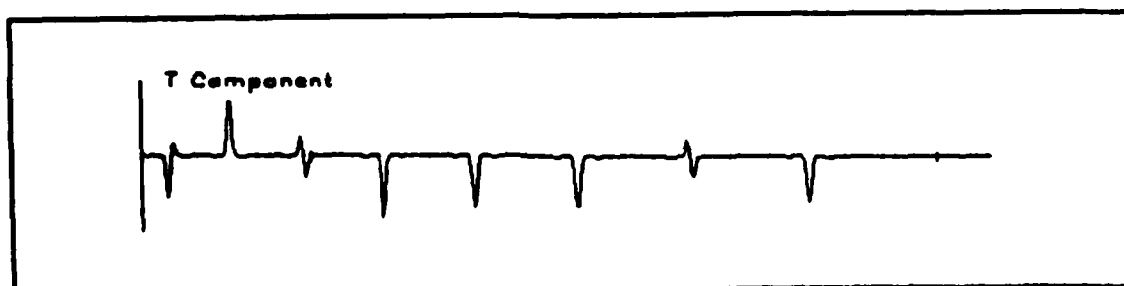
Figure 2: (a) Above: synthetic displacement plot of Lg. Receiver offset is 1000 km. Tick marks in this plot and all synthetic seismograms are at one minute intervals. (b) Below: convolution of the surface displacement with the impulse response of the WWSSN short period seismometer

24
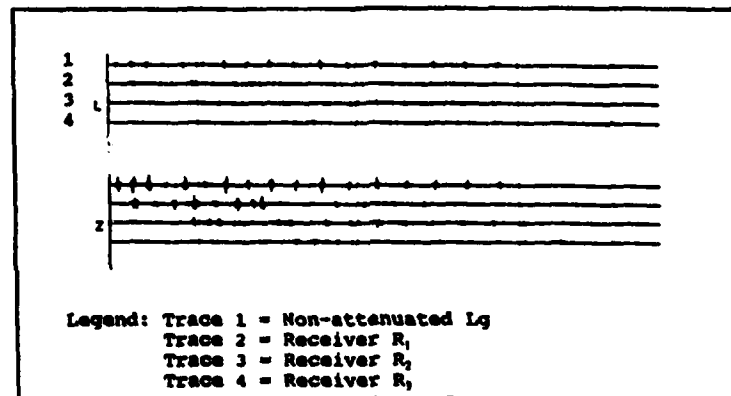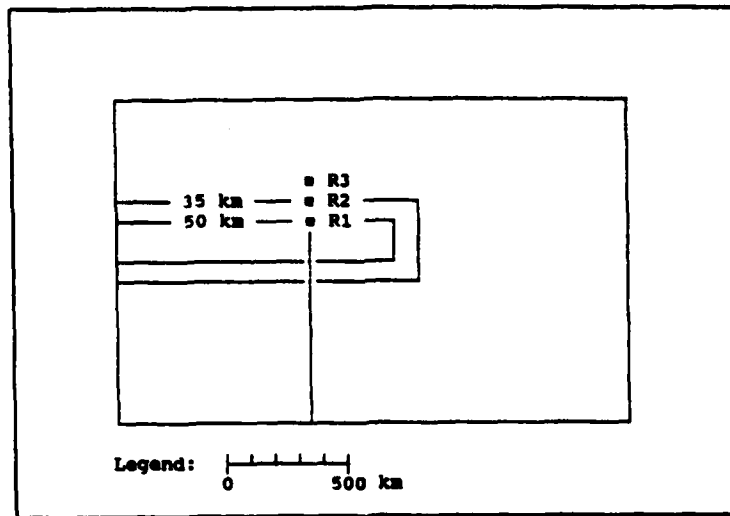
Figure 3: (a) Above: propagation paths normal to strike of mountain range. This map view shows the crustal thickness contours of a narrow hypothetical mountain belt, along with the Lg propagation path and receiver locations. R_1 through R_3 offsets are 2200, 2300, and 2400 km respectively. an unperturbed waveguide. (b) Below: ray synthetic seismograms for paths to receivers R_1 through R_3. Trace 1 is Lg modeled at the R_1 offset in an unperturbed waveguide. Transverse ground motion is not shown because SV to SH conversion does not occur when the propagation path is perpendicular to waveguide variations.

25
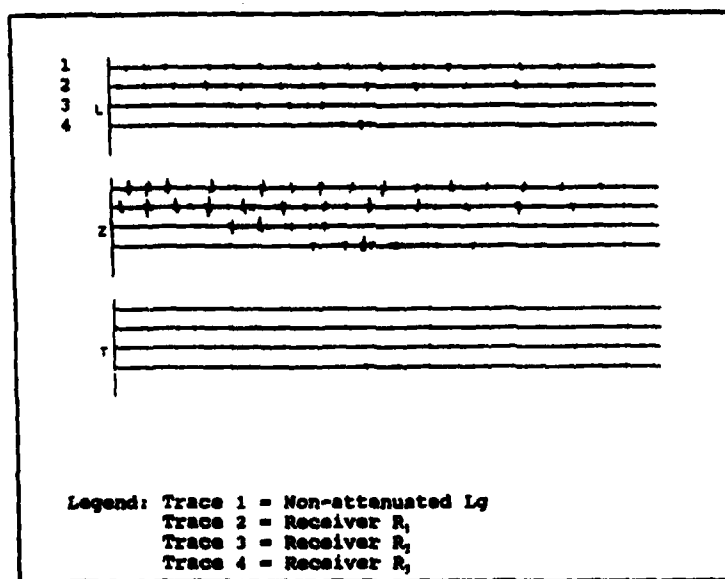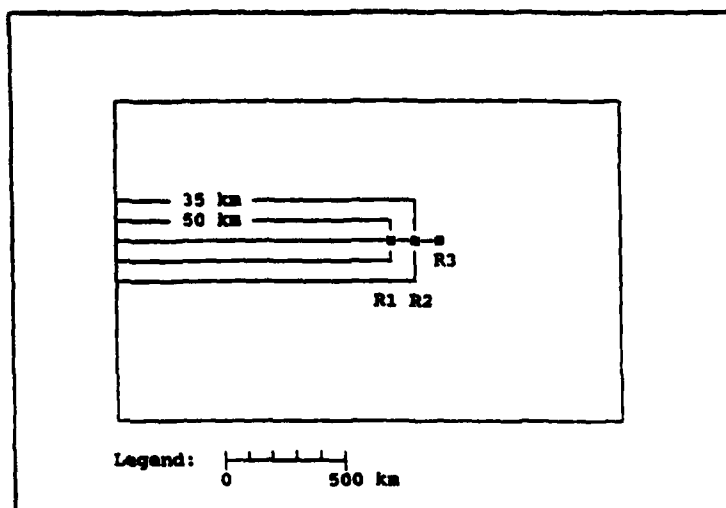
Figure 4: (a) Above: propagation paths parallel to the strike of the mountain range. Offsets are 2200, 2300, and 2400 km. to receivers within the mountain range. (b) Below: ray synthetic seismograms. An increased number of ray paths reach receiver R_1 relative to receivers R_2 and R_3 resulting from lateral reflections within the mountain belt. Coda duration is sharply limited at the R_2 and R_3. Very weak motion can be seen on the transverse traces.
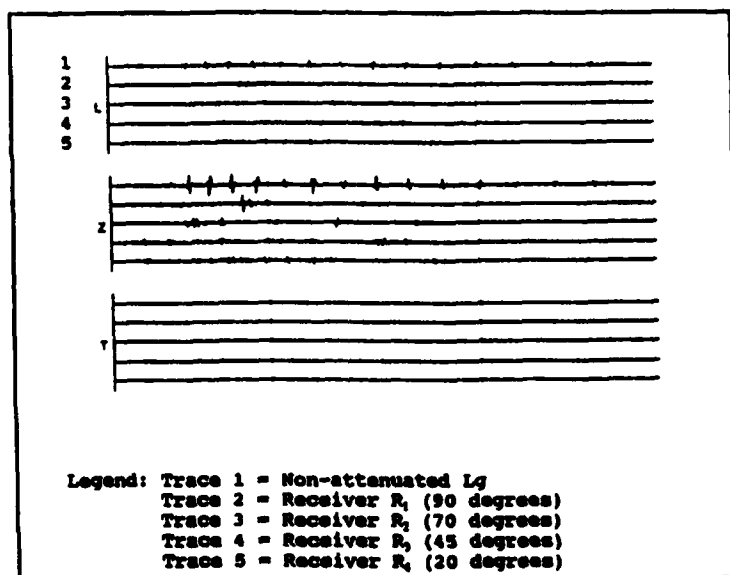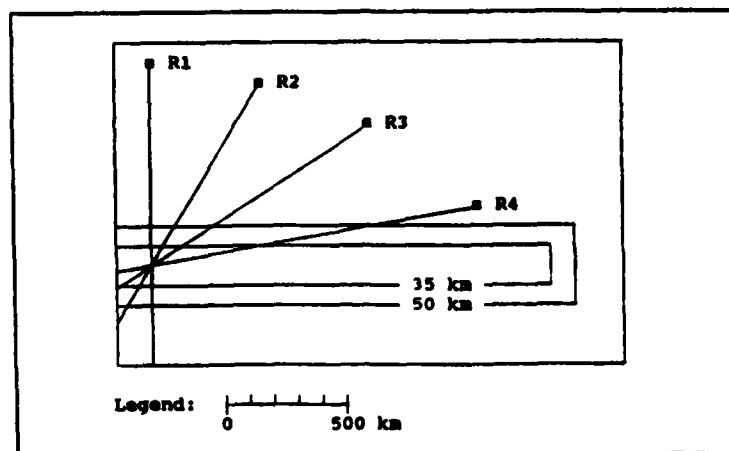
26

Figure 5: Lg propagation at paths making oblique angles to the strike of the mountain range. Above: (a) path to R_1 is at $90°$, path to R_2 is at $70°$, path to R_3 is at $45°$, and path to R_4 is at $20°$. Receiver offset is 2000 km over all paths. Below: (b) ray synthetic seismograms. Although waveforms 2-5 vary considerably, all have been considerably attenuated relative to the reference trace in an unperturbed waveguide and total energy is roughly the same for each of these paths.
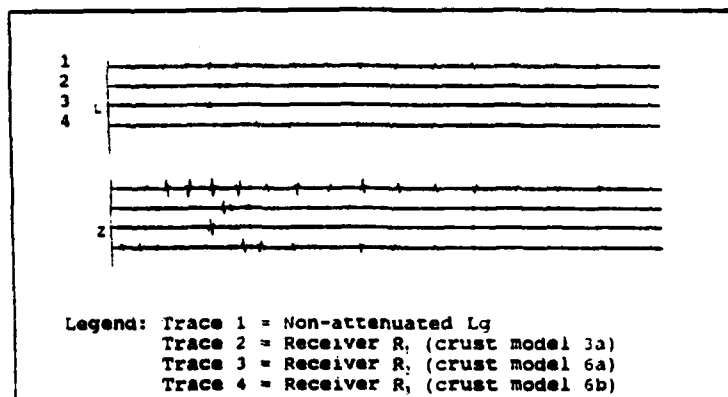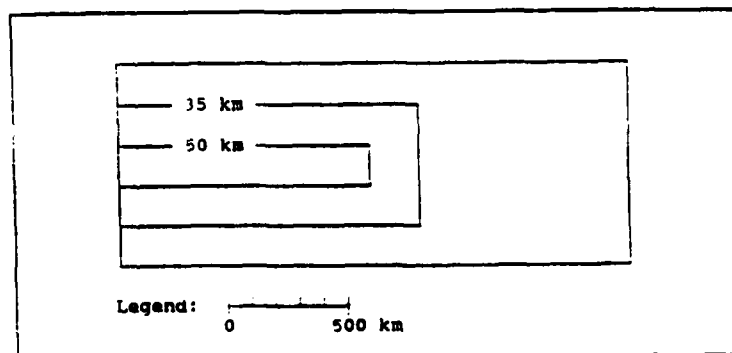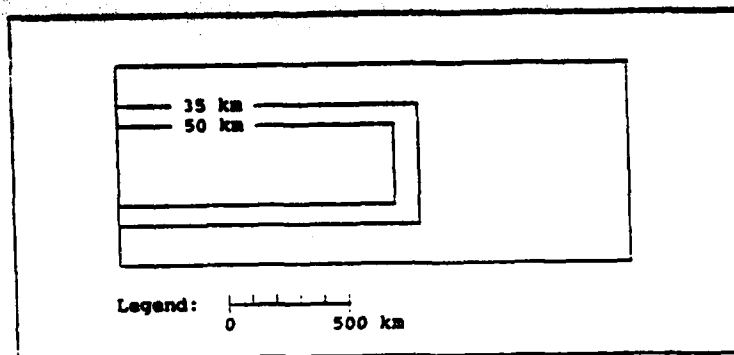
27

Figure 6: Effect of the width of crustal thickening and thinning. The crust increases and decreases in thickness over transition regions 100 km (above) and 200 km (middle). Ray synthetic Lg wavetrains are shown below for an offset of 2000 km and propagation perpendicular to the strike of the mountain range. Weak Lg in traces 2 and 3 compared to strong Lg in trace 4 indicates that the width of the transition region affects Lg efficiency more than the overall width of the mountain root.
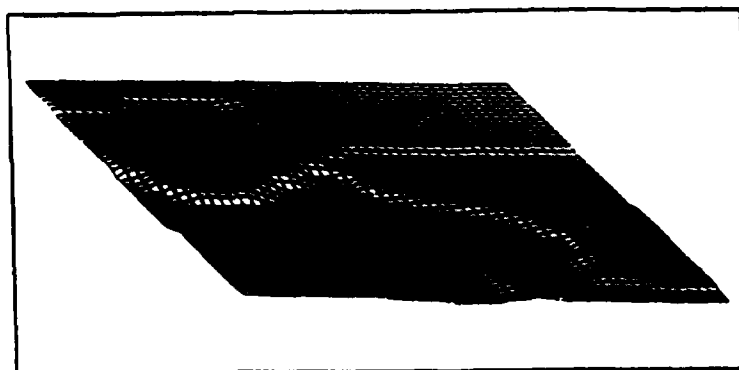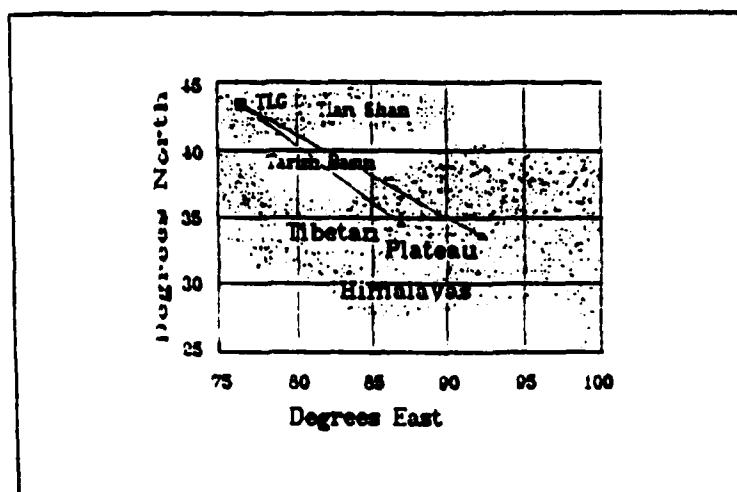
28

Figure 7: Above: (a) map of Central Asia showing the propagation paths of two earthquakes modeled by ray methods. Shading highlights high mountainous regions of thickened crust. The left path gives a detectable Lg signal and is referred to as the strong path. Lg from the right earthquake is very weak. Below: (b) Central Asian Moho depth plot obtained by digitization of crustal thickness values. Not to scale.
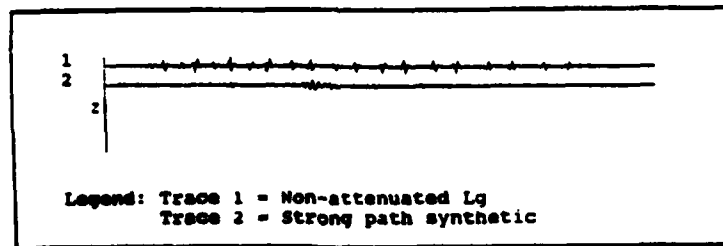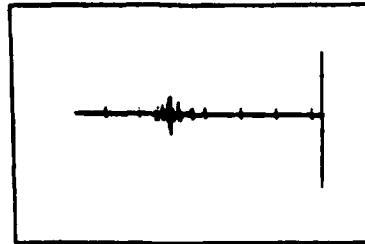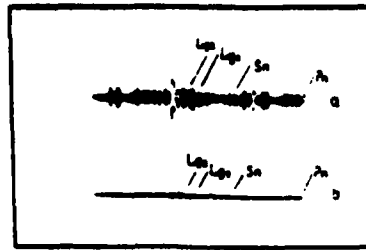
29

Legend: Trace 1 = Non-attenuated Lg
Trace 2 = Strong path synthetic

Figure 8: **Above:** (a) Central Asia strong path seismograms. The seismograms recorded from the left earthquake of Figure 7a show clear Lg energy in both the top trace (instrument response peaked between 0.5 to 1 Hz.) and bottom trace (instrument response peaked between 0.2 to 0.5 Hz.). **Middle:** (b) scaled strong path synthetic. The synthetic seismogram is scaled to the dimensions of the actual seismogram and shows good recreation of Lg. Below (c): detailed strong path synthetic. These synthetic seismograms are not scaled to the recordings and allow determination of the level of attenuation. Ray modeling through a homogeneous crust predicts significant attenuation over this path.

30
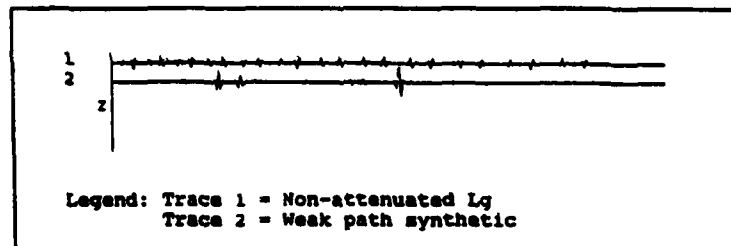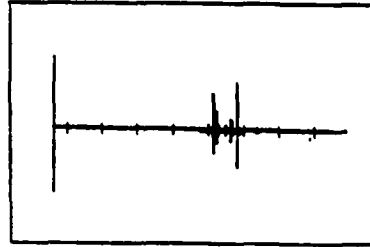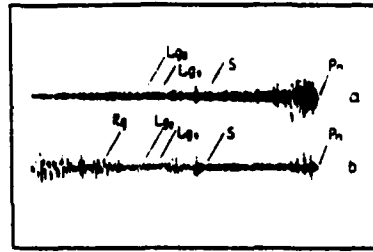
Figure 9: Above: (a) Central Asia weak path seismograms. The seismograms recorded from the right earthquake of Figure 7a show very weak Lg, as can be seen by comparing Lg amplitude to Pn. Middle: (b) scaled weak path synthetic. The synthetic seismogram of the weak path predicts energetic pulses that are not present in the actual recordings. Below: (c) detailed weak path synthetic. Lg is clearly attenuated over this path but, as seen in Figure 9b, the predicted level of attenuation is insufficient to explain the observations.

31

Prof. Thomas Ahrens
Seismological Lab, 252-21
Division of Geological & Planetary Sciences
California Institute of Technology
Pasadena, CA 91125

Prof. Keiiti Aki
Center for Earth Sciences
University of Southern California
University Park
Los Angeles, CA 90089-0741

Prof. Shelton Alexander
Geosciences Department
403 Deike Building
The Pennsylvania State University
University Park, PA 16802

Dr. Ralph Alewine, III
DARPA/NMRO
3701 North Fairfax Drive
Arlington, VA 22203-1714

Prof. Charles B. Archambeau
CIRES
University of Colorado
Boulder, CO 80309

Dr. Thomas C. Bache, Jr.
Science Applications Int'l Corp.
10260 Campus Point Drive
San Diego, CA 92121 (2 copies)

Prof. Muawia Barazangi
Institute for the Study of the Continent
Cornell University
Ithaca, NY 14853

Dr. Jeff Barker
Department of Geological Sciences
State University of New York
 at Binghamton
Vestal, NY 13901

Dr. Douglas R. Baumgardt
ENSCO, Inc
5400 Port Royal Road
Springfield, VA 22151-2388

Dr. Susan Beck
Department of Geosciences
Building #77
University of Arizona
Tuscon, AZ 85721

Dr. T.J. Bennett
S-CUBED
A Division of Maxwell Laboratories
11800 Sunrise Valley Drive, Suite 1450
Reston, VA 22091

Dr. Robert Blandford
AFTAC/TT, Center for Seismic Studies
1330 North 17th Street
Suite 1450
Arlington, VA 22209-2308

Dr. G.A. Bollinger
Department of Geological Sciences
Virginia Polytechnical Institute
21044 Derring Hall
Blacksburg, VA 24061

Dr. Stephen Bratt
Center for Seismic Studies
1300 North 17th Street
Suite 1450
Arlington, VA 22209-2308

Dr. Lawrence Burdick
Woodward-Clyde Consultants
566 El Dorado Street
Pasadena, CA 91109-3245

Dr. Robert Burridge
Schlumberger-Doll Research Center
Old Quarry Road
Ridgefield, CT 06877

Dr. Jerry Carter
Center for Seismic Studies
1300 North 17th Street
Suite 1450
Arlington, VA 22209-2308

Eric Chael
Division 9241
Sandia Laboratory
Albuquerque, NM 87185

Prof. Vernon F. Cormier
Department of Geology & Geophysics
U-45, Room 207
University of Connecticut
Storrs, CT 06268

Prof. Anton Dainty
Earth Resources Laboratory
Massachusetts Institute of Technology
42 Carleton Street
Cambridge, MA 02142

Prof. Steven Day
Department of Geological Sciences
San Diego State University
San Diego, CA 92182

Marvin Denny
U.S. Department of Energy
Office of Arms Control
Washington, DC 20585

Dr. Zoltan Der
ENSCO, Inc.
5400 Port Royal Road
Springfield, VA 22151-2388

Prof. Adam Dziewonski
Hoffman Laboratory, Harvard University
Dept. of Earth Atmos. & Planetary Sciences
20 Oxford Street
Cambridge, MA 02138

Prof. John Ebel
Department of Geology & Geophysics
Boston College
Chestnut Hill, MA 02167

Eric Fielding
SNEE Hall
INSTOC
Cornell University
Ithaca, NY 14853

Dr. Mark D. Fisk
Mission Research Corporation
735 State Street
P.O. Drawer 719
Santa Barbara, CA 93102

Prof Stanley Flatte
Applied Sciences Building
University of California, Santa Cruz
Santa Cruz, CA 95064

Dr. John Foley
NER-Geo Sciences
1100 Crown Colony Drive
Quincy, MA 02169

Prof. Donald Forsyth
Department of Geological Sciences
Brown University
Providence, RI 02912

Art Frankel
U.S. Geological Survey
922 National Center
Reston, VA 22092

Dr. Cliff Frolich
Institute of Geophysics
8701 North Mopac
Austin, TX 78759

Dr. Holly Given
IGPP, A-025
Scripps Institute of Oceanography
University of California, San Diego
La Jolla, CA 92093

Dr. Jeffrey W. Given
SAIC
10260 Campus Point Drive
San Diego, CA 92121

Dr. Dale Glover
Defense Intelligence Agency
ATTN: ODT-1B
Washington, DC 20301

Dr. Indra Gupta
Teledyne Geotech
314 Montgomery Street
Alexanderia, VA 22314

Dan N. Hagedon
Pacific Northwest Laboratories
Battelle Boulevard
Richland, WA 99352

Dr. James Hannon
Lawrence Livermore National Laboratory
P.O. Box 808
L-205
Livermore, CA 94550

Dr. Roger Hansen
AFTAC/TTR
Patrick AFB, FL 32925

Prof. David G. Harkrider
Seismological Laboratory
Division of Geological & Planetary Sciences
California Institute of Technology
Pasadena, CA 91125

2

Prof. Danny Harvey
CIRES
University of Colorado
Boulder, CO 80309

Prof. Donald V. Helmberger
Seismological Laboratory
Division of Geological & Planetary Sciences
California Institute of Technology
Pasadena, CA 91125

Prof. Eugene Herrin
Institute for the Study of Earth and Man
Geophysical Laboratory
Southern Methodist University
Dallas, TX 75275

Prof. Robert B. Herrmann
Department of Earth & Atmospheric Sciences
St. Louis University
St. Louis, MO 63156

Prof. Lane R. Johnson
Seismographic Station
University of California
Berkeley, CA 94720

Prof. Thomas H. Jordan
Department of Earth, Atmospheric &
 Planetary Sciences
Massachusetts Institute of Technology
Cambridge, MA 02139

Prof. Alan Kafka
Department of Geology & Geophysics
Boston College
Chestnut Hill, MA 02167

Robert C. Kemerait
ENSCO, Inc.
445 Pineda Court
Melbourne , FL 32940

Dr. Max Koontz
U.S. Dept. of Energy/DP 5
Forrestal Building
1000 Independence Avenue
Washington, DC 20585

Dr. Richard LaCoss
MIT Lincoln Laboratory, M-200B
P.O. Box 73
Lexington, MA 02173-0073

Dr. Fred K. Lamb
University of Illinois at Urbana-Champaign
Department of Physics
1110 West Green Street
Urbana, IL 61801

Prof. Charles A. Langston
Geosciences Department
403 Deike Building
The Pennsylvania State University
University Park, PA 16802

Prof. Thorne Lay
Institute of Tectonics
Earth Science Board
University of California, Santa Cruz
Santa Cruz, CA 95064

Dr. William Leith
U.S. Geological Survey
Mail Stop 928
Reston, VA 22092

James F. Lewkowicz
Phillips Laboratory/GPEH
Hanscom AFB, MA 01731-5000

Mr. Alfred Lieberman
ACDA/VI-OA State Department Building
Room 5726
320-21st Street, NW
Washington, DC 20451

Prof. L. Timothy Long
School of Geophysical Sciences
Georgia Institute of Technology
Atlanta, GA 30332

Dr. Robert Masse
Denver Federal Building
Bos 25046, Mail Stop 967
Denver, CO 80225

Dr. Randolph Martin, III
New England Research, Inc.
76 Olcott Drive
White River Junction, VT 05001

Dr. Gary McCartor
Department of Physics
Southern Methodist University
Dallas, TX 75275

3

Prof. Thomas V. McEvilly
Seismographic Station
University of California
Berkeley, CA 94720

Prof. John A. Orcutt
IGPP, A-025
Scripps Institute of Oceanography
University of California, San Diego
La Jolla, CA 92093

Prof. Art McGarr
U.S. Geological Survey
Mail Stop 977
U.S. Geological Survey
Menlo Park, CA 94025

Prof. Jeffrey Park
Kline Geology Laboratory
P.O. Box 6666
New Haven, CT 06511-8130

Dr. Keith L. McLaughlin
S-CUBED
A Division of Maxwell Laboratory
P.O. Box 1620
La Jolla, CA 92038-1620

Howard Patton
Lawrence Livermore National Laboratory
L-025
P.O. Box 808
Livermore, CA 94550

Stephen Miller & Dr. Alexander Florence
SRI International
333 Ravenswood Avenue
Box AF 116
Menlo Park, CA 94025-3493

Dr. Frank Pilotte
HQ AFTAC/TT
Patrick AFB, FL 32925-6001

Prof. Bernard Minster
IGPP, A-025
Scripps Institute of Oceanography
University of California, San Diego
La Jolla, CA 92093

Dr. Jay J. Pulli
Radix Systems, Inc.
2 Taft Court, Suite 203
Rockville, MD 20850

Prof. Brian J. Mitchell
Department of Earth & Atmospheric Sciences
St. Louis University
St. Louis, MO 63156

Dr. Robert Reinke
ATTN; FCTVTD
Field Command
Defense Nuclear Agency
Kirtland AFB, NM 87115

Mr. Jack Murphy
S-CUBED
A Division of Maxwell Laboratory
11800 Sunrise Valley Drive, Suite 1212
Reston, VA 22091 (2 Copies)

Prof. Paul G. Richards
Lamont-Doherty Geological Observatory
 of Columbia University
Palisades, NY 10964

Dr. Keith K. Nakanishi
Lawrence Livermore National Laboratory
L-025
P.O. Box 808
Livermore, CA 94550

Mr. Wilmer Rivers
Teledyne Geotech
314 Montgomery Street
Alexandria, VA 22314

Dr. Carl Newton
Los Alamos National Laboratory
P.O. Box 1663
Mail Stop C335, Group ESS-3
Los Alamos, NM 87545

Dr. George Rothe
HQ AFTAC/TTR
Patrick AFB, FL 32925-6001

Dr. Bao Nguyen
AFTAC/TTR
Patrick AFB, FL 32925

Dr. Alan S. Ryall, Jr.
DARPA/NMRO
3701 North Fairfax Drive
Arlington, VA 22209-1714

Dr. Richard Sailor
TASC, Inc.
55 Walkers Brook Drive
Reading, MA 01867

Prof. Charles G. Sammis
Center for Earth Sciences
University of Southern California
University Park
Los Angeles, CA 90089-0741

Prof. Christopher H. Scholz
Lamont-Doherty Geological Observatory
 of Columbia University
Palisades, CA 10964

Dr. Susan Schwartz
Institute of Tectonics
1156 High Street
Santa Cruz, CA 95064

Secretary of the Air Force
(SAFRD)
Washington, DC 20330

Office of the Secretary of Defense
DDR&E
Washington, DC 20330

Thomas J. Sereno, Jr.
Science Application Int'l Corp.
10260 Campus Point Drive
San Diego, CA 92121

Dr. Michael Shore
Defense Nuclear Agency/SPSS
6801 Telegraph Road
Alexandria, VA 22310

Dr. Matthew Sibol
Virginia Tech
Seismological Observatory
4044 Derring Hall
Blacksburg, VA 24061-0420

Prof. David G. Simpson
IRIS, Inc.
1616 North Fort Myer Drive
Suite 1400
Arlington, VA 22209

Donald L. Springer
Lawrence Livermore National Laboratory
L-025
P.O. Box 808
Livermore, CA 94550

Dr. Jeffrey Stevens
S-CUBED
A Division of Maxwell Laboratory
P.O. Box 1620
La Jolla, CA 92038-1620

Lt. Col. Jim Stobie
ATTN: AFOSR/NL
Bolling AFB
Washington, DC 20332-6448

Prof. Brian Stump
Institute for the Study of Earth & Man
Geophysical Laboratory
Southern Methodist University
Dallas, TX 75275

Prof. Jeremiah Sullivan
University of Illinois at Urbana-Champaign
Department of Physics
1110 West Green Street
Urbana, IL 61801

Prof. L. Sykes
Lamont-Doherty Geological Observatory
 of Columbia University
Palisades, NY 10964

Dr. David Taylor
ENSCO, Inc.
445 Pineda Court
Melbourne, FL 32940

Dr. Steven R. Taylor
Los Alamos National Laboratory
P.O. Box 1663
Mail Stop C335
Los Alamos, NM 87545

Prof. Clifford Thurber
University of Wisconsin-Madison
Department of Geology & Geophysics
1215 West Dayton Street
Madison, WS 53706

Prof. M. Nafi Toksoz
Earth Resources Lab
Massachusetts Institute of Technology
42 Carleton Street
Cambridge, MA 02142

Dr. Larry Turnbull
CIA-OSWR/NED
Washington, DC 20505

DARPA/RMO/SECURITY OFFICE
3701 North Fairfax Drive
Arlington, VA 2203-1714

Dr. Gregory van der Vink
IRIS, Inc.
16116 North Fort Myer Drive
Suite 1440
Arlington, VA 22209

HQ DNA
ATTN: Technical Library
Washington, DC 20305

Dr. Karl Veith
EG&G
5211 Auth Road
Suite 240
Suitland, MD 20746

Defense Intelligence Agency
Directorate for Scientific & Technical Intelligence
ATTN: DTIB
Washington, DC 20340-6158

Prof. Terry C. Wallace
Department of Geosciences
Building #77
University of Arizona
Tuscon, AZ 85721

Defense Technical Information Center
Cameron Station
Alexandria, VA 22314 (5 Copies)

Dr. Thomas Weaver
Los Alamos National Laboratory
P.O. Box 1663
Mail Stop C335
Los Alamos, NM 87545

TACTEC
Battelle Memorial Institute
505 King Avenue
Columbus, OH 43201 (Final Report)

Dr. William Wortman
Mission Research Corporation
8560 Cinderbed Road
Suite 700
Newington, VA 22122

Phillips Laboratory
ATTN: XPG
Hanscom AFB, MA 01731-5000

Prof. Francis T. Wu
Department of Geological Sciences
State University of New York
 at Binghamton
Vestal, NY 13901

Phillips Laboratory
ATTN: GPE
Hanscom AFB, MA 01731-5000

AFTAC/CA
(STINFO)
Patrick AFB, FL 32925-6001

Dr. Michel Bouchon
I.R.I.G.M.-B.P. 68
38402 St. Martin D'Heres
Cedex, FRANCE

DAARPA/PM
3701 North Fairfax Drive
Arlington, VA 22203-1714

Dr. Michel Campillo
Observatoire de Grenoble
I.R.I.G.M.-B.P. 53
38041 Grenoble, FRANCE

DARPA/RMO/RETRIEVAL
3701 North Fairfax Drive
Arlington, VA 22203-1714

Dr. Kin Yip Chun
Geophysics Division
Physics Department
University of Toronto
Ontario, CANADA

6

Prof. Hans-Peter Harjes
Institute for Geophysics
Ruhr University/Bochum
P.O. Box 102148
4630 Bochum 1, GERMANY

Prof. Eystein Husebye
NTNF/NORSAR
P.O. Box 51
N-2007 Kjeller, NORWAY

David Jepsen
Acting Head, Nuclear Monitoring Section
Bureau of Mineral Resources
Geology and Geophysics
G.P.O. Box 378, Canberra, AUSTRALIA

Ms. Eva Johannisson
Senior Research Officer
National Defense Research Inst.
P.O. Box 27322
S-102 54 Stockholm, SWEDEN

Dr. Peter Marshall
Procurement Executive
Ministry of Defense
Blacknest, Brimpton
Reading FG7-FRS, UNITED KINGDOM

Dr. Bernard Massinon, Dr. Pierre Mechler
Societe Radiomana
27 rue Claude Bernard
75005 Paris, FRANCE (2 Copies)

Dr. Svein Mykkeltveit
NTNT/NORSAR
P.O. Box 51
N-2007 Kjeller, NORWAY (3 Copies)

Prof. Keith Priestley
University of Cambridge
Bullard Labs, Dept. of Earth Sciences
Madingley Rise, Madingley Road
Cambridge CB3 OEZ, ENGLAND

Dr. Jorg Schlittenhaardt
Federal Institute for Geosciences & Nat'l Res.
Postfach 510153
D-3000 Hannover 51, GERMANY

Dr. Johannes Schweitzer
Institute of Geophysics
Ruhr University/Bochum
P.O. Box 1102148
4360 Bochum 1, GERMANY